An integrated approach to local ultrasonic monitoring of fastener hole fatigue cracks

A. C. Cobb
Southwest Research Institute
San Antonio
Texas
USA

J. E. Michaels and T. E. Michaels
jennifer.michaels@ece.gatech.edu
School of Electrical and Computer Engineering,
Georgia Institute of Technology
Atlanta, Georgia
USA

ABSTRACT

Ultrasonic nondestructive evaluation methods are routinely used to detect and size fatigue cracks near fastener holes in aircraft structures as a part of scheduled maintenance. In contrast, statistical crack propagation models provide an estimate of the expected fatigue life assuming a known crack size and future fatigue loadings. Here an integrated approach for *in situ* diagnosis and prognosis of fastener hole fatigue cracks is proposed and implemented that incorporates both ultrasonic monitoring and crack growth laws. The sensing method is an ultrasonic angle beam technique, and cracks are automatically detected from the ultrasonic response. An extended Kalman filter is applied to combine ultrasonically estimated crack sizes with a crack growth law, effectively using the time history of the ultrasonic results rather than only the most recent measurement. A natural extension of this method is fatigue life prognosis. Results from fatigue tests on 7075-T651 aluminium coupons show improved crack size estimates as compared to those obtained from ultrasonic measurements alone, and also demonstrate the capability of predicting the remaining life. This approach for fatigue crack detection, sizing and prognosis is an example of a general strategy for *in situ* monitoring of structural damage whereby improved results are achieved from the integration of noisy measurements with imperfect crack growth models.

NOMENCLATURE

a	crack depth in mm, same as x
$\hat{a}$	measurement system response, $1 - \bar{R}$
$A(x)$	system model for evolving crack depth x
$\bar{A}(n)$	linearised system model at measurement set n
$B(x)$	measurement model giving normalised energy ratio $\bar{R}$ as a function of crack depth x
$\bar{B}(n)$	linearised measurement model at measurement set n
$\tilde{B}(\bar{R})$	inverse measurement model giving crack depth x as a function of normalised energy ratio $\bar{R}$
c_0	linear fit parameter
c_1	linear fit parameter
C	multiplicative material constant for Paris's Law
$E(n, L)$	energy of the ultrasonic waveform after the nth measurement set and at an externally applied load of L
F	geometry correction factor for Paris's Law
$G(n)$	Kalman gain for measurement set n
h	specimen thickness
k_T	stress concentration factor
L	externally applied load
L_{ref}	reference load necessary to fully open cracks
m	exponential material constant for Paris's Law
M	number of measurements in the prediction set for the crack

Paper No. 3315. Manuscript received 10 July 2008, accepted 28 August 2008.

https://doi.org/10.1017/S0001924000003432 Published online by Cambridge University Press

	detection algorithm
n	measurement set number
n_c	current measurement set
n_{detect}	measurement set when cracking is detected
N	number of measurements between the prediction set and the current measurement for the crack detection algorithm
N_f	number of fatigue cycles
$P(n)$	predicted error covariance at measurement set n
Q	shape variable for geometry correction factor, F
Q_v	variance of measurement model Gaussian noise $v(n)$
Q_w	variance of system model Gaussian noise $w(n)$
Q_Ω	variance of log-normal distribution, Ω
r	radius of fastener hole
$R(n)$	raw (unnormalised) ultrasonic energy ratio at measurement set n
$\bar{R}(n)$	normalised energy ratio at measurement set n
$s(t; n,L)$	ultrasonic waveform at measurement set n and externally applied load L
t	time of flight of the ultrasonic signal
t_{max}	maximum time for ultrasonic waveform energy integral
t_{min}	minimum time for ultrasonic waveform energy integral
$v(n)$	additive Gaussian noise for the measurement model, $B(x)$
$w(n)$	additive Gaussian noise for the system model, $A(x)$
$x(n)$	crack depth at measurement set n, same as a
$\hat{x}(n \mid m)$	estimate of crack depth at measurement set n using measurements up to set m ($m \le n$)
$y(n)$	normalised energy ratio measurement at measurement set n, same as $\bar{R}(n)$
$\hat{y}(n)$	estimate of $\bar{R}(n)$ based upon $\hat{x}(n \mid n-1)$
ΔK	stress intensity range
ΔK_i	stress intensity range for the ith cycle of the fatigue spectrum
ΔK_f	number of fatigue cycles between measurements
ΔS	applied stress range
v	normal random variable for the distribution of $\hat{a}$ *versus* a
σ_v	standard deviation of measurements from linear fit in log-log domain
σ_e^2	variance contribution of $w(n)$ from experimental sources
Ω	log-normal distribution for multiplicative material constant

1.0 INTRODUCTION

Fatigue cracks originating from fastener holes have been studied extensively because of their importance in determining the remaining life of aerospace structures. Currently, the maintenance of many airframes is based upon statistical modelling of crack growth within aircraft structures[1,2]. Statistical approaches alone do not take into account the actual state of the structure, typically leading to overly conservative life estimation. On the other hand, there are many ultrasonic nondestructive inspection techniques for the detection and sizing of defects. However, these measurement-based techniques largely ignore the physics of fatigue crack propagation, producing life estimates using only the most recent ultrasonic measurement. The primary objective of this paper is to provide an integrated structural health monitoring (SHM) framework for estimating the size of fastener hole fatigue cracks in aluminium specimens. A prognosis methodology is also incorporated for determining the remaining life. The overall approach is divided into three parts: detection, tracking and prognosis. An automated algorithm is applied for crack detection, a state estimation technique is employed to track defect growth after detection, and a prognosis strategy is implemented in parallel with tracking to provide a real-time estimate of remaining life.

There is a long history of using ultrasonic methods for crack sizing in the context of nondestructive testing. The idea of an equivalent flaw size is based upon correlating the amplitude of a reflected ultrasonic echo to the size of a standard calibration reflector such as a flat bottom hole[3]. Time-based methods, which have the advantage of being insensitive to unavoidable amplitude variations, are also in common use. The time-of-flight diffraction (TOFD) method is based upon detecting echoes diffracted from crack tips and using the times of the echoes to estimate crack sizes[4,5]. The times of surface waves that have travelled along the crack itself are also used for defect sizing[6]. All of these methods are typically applied in the context of nondestructive evaluation (NDE) whereby transducers are manually or automatically moved to optimise the flaw signals.

More recently, ultrasonic methods using permanently attached transducers have been applied for *in situ* monitoring of fatigue cracks. Cook and Berthelot[7] relate the change in amplitude of a backscattered surface wave to the size of a surface breaking crack. Keller and Ray[8] utilise an ultrasonic angle beam through-transmission method and empirically relate the loss in received energy to crack length. Mi *et al*[9] apply a similar ultrasonic angle beam configuration optimized for smaller cracks, and utilise dynamic load modulations for crack detection and sizing. Kim *et al*[10] use load-modulated surface waves for *in situ* crack detection and sizing. Harri *et al*[11] generate surface waves using a multi-frequency sine wave and relate the frequency-dependent response to crack depth. All of these *in situ* methods either assume that cracks are open or rely explicitly upon applied loads to open the cracks; it is well-known that closed or partially closed cracks can be very difficult to detect ultrasonically.

Lamb wave methods have also been proposed for *in situ* monitoring of fatigue cracks. Chang and Mal[12] compare experimental and numerical signals and spectra for the S_0 mode interacting with small EDM through-thickness notches (1·6mm and 3·2mm in length) emanating from a hole. Fromme and Sayir[13] show that the A_0 mode scattered from a fastener hole with a through-thickness notch is sensitive to crack lengths substantially smaller than the incident wavelength. Other Lamb wave studies of fatigue crack detection also consider through-thickness cracks and notches, but of generally larger lengths; e.g., Refs 14-16. Michaels *et al*[17] consider detection of much smaller fastener hole cracks that are not surface-breaking, but were not able to conclusively detect cracks of this size using the S_0 Lamb wave mode.

For ultrasonic monitoring applications it is not possible to move transducers as is done for NDE, but unlike NDE, time history data are available. Keller and Ray[8] estimate a crack growth model parameter from the time history of empirically determined ultrasonic crack sizes, and the resulting model is used to predict subsequent crack growth. Cobb *et al*[18] perform a trend analysis on an ultrasonic feature to automatically detect the onset of cracking. Gupta *et al*[19-20] apply symbolic time series analysis methods to ultrasonic signals for early detection of damage. It is difficult to find other examples in the literature where ultrasonic time history data from monitoring of fatigue cracks is used in ways other than to display results as a function of time.

Stochastic modelling of fatigue crack dynamics, including a generic measurement model, was proposed by Ray and Tangirala[21], but their work did not include sensor data. Orchard and Vachtsevanos[22] apply a particle-filtering approach to combine a measurement model for vibration data with a crack propagation model to implement fault diagnosis and prognosis for a planetary gear plate. Kulkarni *et al*[23,24] consider an integrated probabilistic methodology that uses nonlinear ultrasonic data in the pre-macro-crack regime and ultrasonic (or other) inspection data after a macro crack has initiated. Their work further assumes that crack growth models are available for both regimes, and proof-of-concept results are presented using simulated crack growth and measurement data. The approach taken in the work reported here is similar in concept to the strategies of Refs 21 and 22 in that a state estimation method is used to combine measurement-based crack size estimates with a crack propagation model. This approach explicitly takes into account the inaccuracies of both the measurement method and the crack growth model by incorporating variances of both into the state estimation process.

https://doi.org/10.1017/S0001924000003432 Published online by Cambridge University Press

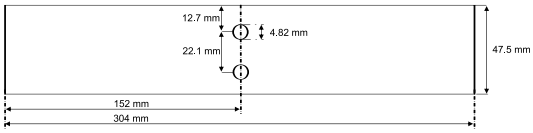

Figure 1. Two-hole fatigue coupon with a thickness of 5·72mm (drawing not to scale).

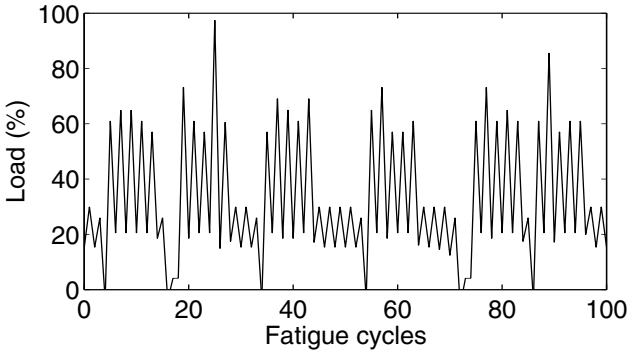

Figure 2. Representative segment of the fatigue loading spectrum.

The paper is organised as follows. Section 2 describes the fatigue tests, ultrasonic method and analysis algorithms. Section 3 explains the approach taken for crack detection, crack size estimation, and prognosis. Experimental results are reported and discussed in Section 4 and concluding remarks are made in Section 5.

2.0 EXPERIMENTS

The purpose of the experiments is to generate fatigue cracks originating from through-holes that are monitored using permanently attached ultrasonic transducers. Ultrasonic waveforms are captured throughout the fatiguing process and are analysed in real-time. The analysis is based upon a load-dependent energy feature that is directly related to the presence and degree of fatigue cracking originating from the through-hole. The specimen properties and geometry, the fatiguing process, the ultrasonic technique, and the ultrasonic feature for subsequent analysis are briefly described in this section. Additional details may be found in Refs 9, 18, 25 and 26.

2.1 Specimen properties and geometry

The specimens examined in this study were manufactured from 7075-T651 aluminium with two through-holes in the centre of the sample as shown in Fig. 1. The through-holes are meant to represent fastener holes by acting as stress risers for crack formation. The hole and specimen geometries are such that stresses on either side of the hole are approximately equal, and the hole separation is sufficient so that each of the two holes can be considered to be independent with respect to crack initiation and growth.

2.2 Fatigue process

All samples were fatigued at 5Hz by repeating a purely tension, 2,640 cycle spectrum using a commercial fatigue machine. A representative section of the fatigue spectrum is shown in Fig. 2. As shown, the spectrum is divided into high and low stress packets, with 70% of the cycles considered low stress. The peak loading of the spectrum is approximately 77,840N, corresponding to a stress of 284MPa away from the hole, which is approximately 60% of the yield stress. This spectrum is intended to replicate the aperiodic loading experienced by a wing panel fastener hole during service of a military aircraft[27]. Fatiguing was terminated for the majority of the specimens prior to fracture to assess the small crack performance of the ultrasonic method. Final crack sizes were determined by fracturing the sample after testing was ended and measuring the crack dimensions from photographs of the fracture surfaces. Additional specimens were fatigued to failure to evaluate the prognosis method.

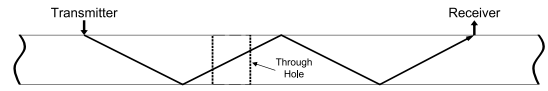

Figure 3. Double V (double skip) beam path for monitoring the hole for fatigue cracks using angle beam transducers.

2.3 Ultrasonic technique

The method for ultrasonic monitoring of the fastener holes is to bond a pair of angle beam transducers on opposite sides of the hole with the direction of propagation parallel to the loading axis[9]. This angle beam through transmission configuration allows a bulk shear wave to propagate between the transmitter and receiver via reflections between the top and bottom surfaces of the sample. Given the uniaxial fatigue process and known stress concentrations near the hole, the predominant direction of crack growth is perpendicular to the loading direction and no cracking is expected to occur elsewhere. Since the crack location is known, the purpose of this through-transmission approach is detection and characterisation as opposed to localisation.

Figure 3 illustrates one possible transducer configuration. In this figure, the transmitter is positioned such that there is a single boundary reflection before the wave reaches the hole. The direct path from transmitter to receiver is blocked by the hole; the wave is diffracted around the hole where cracks are most likely to initiate. The receive transducer is positioned on the opposite side of the hole at a distance corresponding to three boundary refections of the centre of the beam from the transmitter to the receiver (two full skips, or V paths). For the configuration of Fig. 3, the centre of the beam passes through the centre of the specimen at the location where the wave diffracts around the cylindrical surface of the hole. Variations of this configuration were also employed where the number of V paths and the transducer locations were modified. Prior to mounting the transducers, their actual refracted angles in 7075-T651 aluminium were measured from a corner reflector to enable their nominal locations to be calculated.

The transducers used in this research are commercially available miniature shear wave transducers. The centre frequency of the probes is 10MHz, with a corresponding shear wavelength in aluminium of approximately 0·3mm, to ensure that the inspection wavelength is smaller than the target crack size of 0·5mm. Note that this size is the crack depth as measured from the surface of the fastener hole, which, for a half-penny shaped crack originating at the hole surface midway through the plate thickness, corresponds to a length of 1mm on the surface of the hole. The shear wave method was chosen rather than a lower frequency guided wave method because of the small size of the defects that were targeted for detection; as previously noted, prior guided wave work for fatigue crack detection primarily considered through-thickness cracks, which are not the case here. A laboratory pulser-receiver was used to generate a spike excitation pulse for the transmitting transducer, and

https://doi.org/10.1017/S0001924000003432 Published online by Cambridge University Press

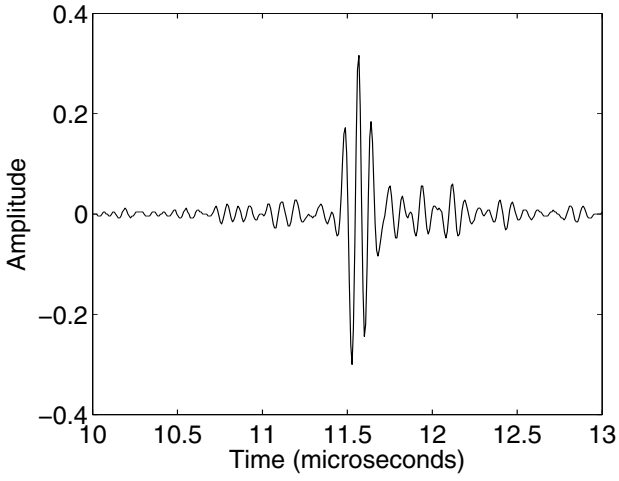

Figure 4. Example through transmission ultrasonic waveform.

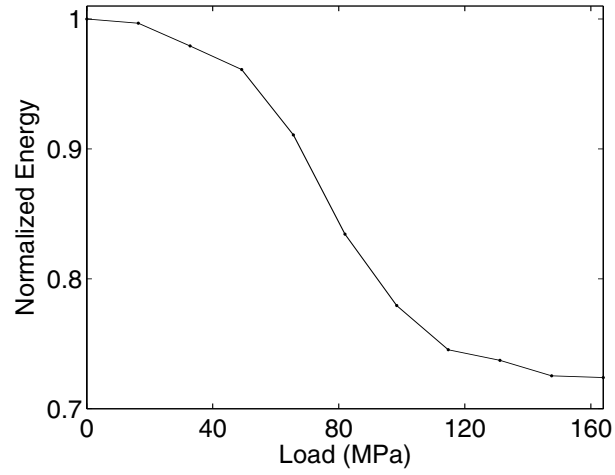

Figure 5. Energy *versus* load curve that is typical for a non-surface-breaking crack with a depth of approximately 0·5mm.

a digital oscilloscope recorded the resulting waveform at the receive transducer. An example waveform from an uncracked specimen is shown in Fig. 4.

The nominal measurement schedule for the ultrasonic signals was to record waveforms after every 1,320 fatigue cycles, although some data were recorded at different intervals. Data acquisition continued on a predetermined schedule until the termination of fatiguing. The waveforms were either captured while fatiguing was paused at eleven static load levels from 0 to 44,482N (164MPa) in 4,448N (16·4GPa) increments, or dynamically during fatiguing with the loads estimated from the time shifts of the ultrasonic signals[9]. The dynamic method was developed both to facilitate data acquisition by not requiring interruption of the fatigue process and to provide a means of implementing the ultrasonic method under the variable loading conditions experienced during flight. The ultrasonic method has been successfully applied to full scale fatigue tests with data acquired using this dynamic method[28].

2.4 Waveform analysis

The ultrasonic waveform feature used for data analysis is a ratio of signal energies from samples under tensile loading to their unloaded counterparts normalised by the ratio from the undamaged specimen, which is discussed in the previous work by the authors[9]. It is thus a measure of the load-dependent ultrasonic response primarily caused by cracks opening with load. The energy in a specified time window for a given number of fatigue cycles and load level is calculated as

$$E(n,L)=\int_{t_{min}}^{t_{max}} s^2(t;n,L)\mathrm{d}t, \qquad \ldots (1)$$

where this equation is given in continuous time for clarity. Here $s(t;n,L)$ is the waveform from the nth ultrasonic measurement set and with an applied load of L, and the total time window considered is from t_{min} to t_{max}, defined here to be a 6μs window centred at the largest amplitude arrival. The first measurement set (n = 1) occurs immediately before fatiguing begins. Subsequent measurement sets are recorded at a regular interval, nominally 1,320 cycles, to simplify experimental procedures; however, the presented SHM framework can also be used for a nonuniform measurement interval.

A reference load is selected to be large enough to ensure that any cracks are fully open when this load is applied. A typical plot of energy versus load is shown in Fig. 5 for a specimen with a crack. It can be seen that the energy reaching the receive transducer decreases as the load increases from zero to about 120MPa and remains essentially constant thereafter, indicating that the crack is fully opened. Thus, a reference load of 164MPa is more than sufficient to open this crack; prior experience has shown that this loading is generally effective for fully opening cracks of various sizes and locations[25].

The raw energy ratio, $R(n)$, is calculated as the ratio of the signal energy recorded at the reference load (L_{ref} = 164MPa) to the signal energy at zero load,

$$R(n)=\frac{E(n,L_{ref})}{E(n,0)}. \qquad \ldots (2)$$

It is then normalised by the initial value from the undamaged specimen,

$$\bar{R}(n)=\frac{R(n)}{R(1)}. \qquad \ldots (3)$$

This normalised energy ratio can then be examined as a function of fatigue cycles, where the indication of cracking is a drop in the curve of $\bar{R}$ *vs* n.

3.0 METHODOLOGY

The overall methodology consists of crack detection, crack sizing, and prognosis of remaining life, which are described in the following sections.

3.1 Crack detection

The authors have previously developed an algorithm for detecting defects based upon a time series of $\bar{R}(n)$, the normalised energy ratio[18]. An example curve is shown in Fig. 6, where it can be seen that the energy ratio is relatively flat until cracks are detected, at which point it begins to regularly decline. The basis of the crack detection algorithm is to compare the current energy ratio to a value predicted from a set of prior energy ratio measurements. This procedure is illustrated in Fig. 7 for an example energy ratio curve. Let M be the number of measurements sets that are used for the prediction, referred to as the prediction set. The prediction set is assumed to be representative of the sample without damage. There is a gap of N measurements between the prediction set and the current measurement, n_c, to allow any small cracks to have N measurements in which to propagate prior to detection. In Fig. 7, M = 6 and N = 2.

https://doi.org/10.1017/S0001924000003432 Published online by Cambridge University Press

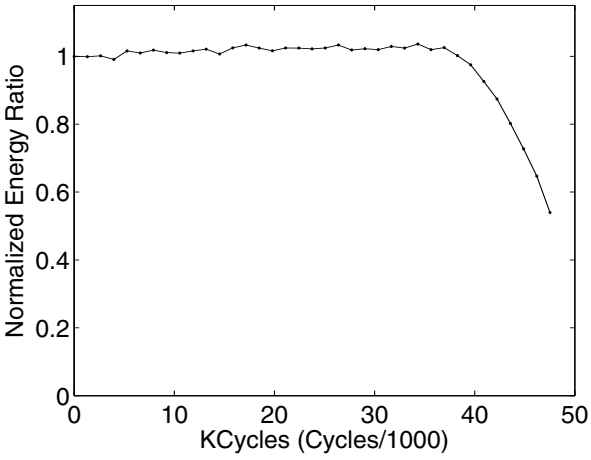

Figure 6. Example of a normalised energy ratio curve.

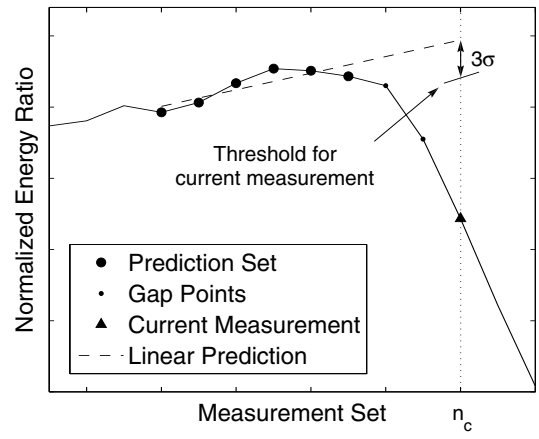

Figure 7. Illustration of the crack detection algorithm with $M = 6$ and $N = 2^{(18)}$.

Now consider a local linear fit of the energy ratio curve using the prediction set, and let σ_e be the calculated standard deviation of the error between the points in the prediction set and the linear fit. A defect is said to be detected if the actual energy ratio at the current measurement, $\bar{R}(n_c)$, is at least three standard deviations ($3\sigma_e$) below the linear prediction. If this drop occurs, the crack detection output, n_{detect}, is the current measurement, n_c, and the future energy ratio measurements ($\bar{R}(n)$ for $n > n_{detect}$) are used to estimate the size of the growing cracks. Also, the σ_e value at detection is the best estimate of the experimental measurement variations; this value is used as part of the defect tracking procedure of Section 3.2.

The prediction set initially comprises the first M measurements of the energy ratio curve, where the assumption is necessarily made that no cracking has occurred within this set. Therefore, the first point at which a crack can be detected is measurement set $M + 1$. The same initial prediction set of M measurements is used for analysing measurements $M + 1$ to $M + N$. For $n_c > M + N$, the prediction set of M points slides forward in time, keeping a gap of N measurements. For a measurement interval of 1,320 cycles, values of $M = 15$ (19,800 cycles) and $N = 2$ (2,640 cycles) were found to give reasonable detection results compared to manual interpretation of the energy ratio curves. For different measurement intervals, M and N were adjusted accordingly.

3.2 Defect tracking

After crack detection, ultrasonic energy ratio measurements are combined with crack growth laws to provide an estimate of the current crack depth. There exist numerous strategies, known collectively as state estimation, for providing an optimal estimate of an evolving parameter by combining a history of measurements with approximate theoretical models. For the work presented in this paper, a classical approach for state estimation, the well-known Kalman Filter, is used to provide a real-time estimate of the crack depth after each energy ratio measurement. A summary of the Kalman filter approach and descriptions of the necessary measurement and crack growth models are provided here.

3.2.1 Kalman filter

There are inherent inaccuracies in any measurement model or system model. Bayesian estimation is a fundamental method for reducing these inaccuracies but it is generally impossible to implement because all needed statistics of the models are typically unknown[29]. For a practical implementation, simplifying assumptions have to be made, such as model linearity and additive Gaussian noise.

The state estimation approach for the work presented here, which combines ultrasonic measurements with a fatigue crack growth power law, is a modification of a basic Kalman filter. A basic Kalman filter requires linear measurement and system models, which are not the case for this application since both models are nonlinear. The extended Kalman filter (EKF) used here is an approximation of a basic Kalman filter that allows for nonlinear measurement and system models via local linearisations of these models about the current state estimate[29,30].

As a summary of the EKF implementation, first consider a nonlinear discrete-time system of the form

$$x(n+1) = A(x(n)) + w(n), \quad \ldots (4)$$

$$y(n) = B(x(n)) + v(n). \quad \ldots (5)$$

For this study, the state variable, x, is the crack depth and the measurement, y, is the normalised ultrasonic energy ratio, $\bar{R}(n)$. The system model, $A(x)$, determines a new crack depth based upon the previous crack depth and the known loading history. The observation (or measurement) function, $B(x)$, determines the expected ultrasonic energy ratio given a specific crack size. Both of these models are nonlinear. The noise functions, w and v, are assumed to be zero-mean Gaussian with variances Q_w and Q_v, respectively, where each noise term is uncorrelated among its samples.

The initial estimate from the EKF at time n is given as

$$\hat{x}(n \mid n-1) = A(\hat{x}(n-1 \mid n-1)). \quad \ldots (6)$$

This crack size estimate is simply the predicted crack size given the previous crack size, $\hat{x}\ (n-1 \mid n-1)$, and the known loading. This prediction is then corrected using the next measurement, $y(n)$,

$$\hat{x}(n \mid n) = \hat{x}(n \mid n-1) + G(n)[y(n) - \hat{y}(n)], \quad \ldots (7)$$

$$\hat{y}(n) = B(\hat{x}(n \mid n-1)), \quad \ldots (8)$$

where $\hat{y}\ (n)$ is the estimate of the measurement based upon $\hat{x}(n \mid n-1)$ and $G(n)$ is the Kalman gain.

The Kalman gain term is related to the predicted error covariance, $P(n)$. The error covariance is determined recursively as

https://doi.org/10.1017/S0001924000003432 Published online by Cambridge University Press

Table 1
Summary of fatigue test data

Experiment	$\bar{R}$	Depth (mm)	Experiment	$\bar{R}$	Depth (mm)
1	0·939	0·082	20	0·862	0·327
2	0·972	0·057	21	0·938	0·214
3	0·967	0·110	22	0·810	0·411
4	0·731	0·605	23	0·927	0·198
5	0·616	0·413	24	0·930	0·253
6	0·879	0·790	25	0·611	0·434
7	0·644	0·415	26	0·456	0·796
8	0·856	0·216	27	0·582	1·005
9	0·840	0·302	28	0·667	0·447
10	0·041	2·558	29	0·435	0·822
11	0·411	1·258	30	0·668	0·449
12	0·716	0·397	31	0·610	0·445
13	0·907	0·298	32	0·536	0·623
14	0·405	0·950	33	0·716	0·440
15	0·919	0·354	34	0·557	0·884
16	0·888	0·475	35	0·870	0·220
17	0·286	0·679	36	0·919	0·315
18	0·747	0·888	37	0·879	0·271
19	0·913	0·320			

$$P(n\,|\,n-1) = \bar{A}(n-1)P(n-1\,|\,n-1)\bar{A}(n-1) + Q_w, \quad \ldots (9)$$

$$G(n) = P(n\,|\,n-1)\bar{B}(n)[\bar{B}(n)P(n\,|\,n-1)\bar{B}(n) + Q_v], \quad \ldots (10)$$

$$P(n\,|\,n) = [1 - G(n)\bar{B}(n)]P(n\,|\,n-1), \quad \ldots (11)$$

where $\bar{A}(n-1)$ and $\bar{B}(n)$ are the linearised system and measurement models,

$$\bar{A}(n-1) = \frac{\partial A(x)}{\partial x}\Big|_{x=\hat{x}(n-1|n-1),} \quad \ldots (12)$$

$$\bar{B}(n) = \frac{\partial B(x)}{\partial x}\Big|_{x=\hat{x}(n|n-1).} \quad \ldots (13)$$

These linearisations are based on first order Taylor series expansions of $A(x)$ and $B(x)$.

For this application, the EKF framework is employed after detection using the crack detection algorithm of Section 3.1. The Kalman filter is initialised based upon the normalised energy ratio from the ultrasonic measurement just prior to detection, $\bar{R}(n_{detect} - 1)$. Let $x = \tilde{B}(\bar{R})$ be the inverse of the measurement model of Equation (8). The initialisation of the Kalman filter is given by

$$\hat{x}(n_{detect} - 1\,|\,n_{detect} - 1) = \tilde{B}(\bar{R}(n_{detect} - 1)), \quad \ldots (14)$$

$$P(n_{detect} - 1\,|\,n_{detect} - 1) = \hat{x}(n_{detect} - 1\,|\,n_{detect} - 1)^2. \quad \ldots (15)$$

3.2.2 Measurement model

The first modelling aspect is determining the relationship between the ultrasonic measurement response and crack depth; this relationship is the measurement model for the EKF. Given the complexity of the ultrasonic energy diffracting around the surface of the hole and interacting with multiple cracks, an empirical approach was employed for approximating this relationship. A series of fatigue tests was performed over several years using the procedure described in the prior sections. Table 1 summarises the energy ratio response and crack depth for 37 individual holes for which cracks were detected. The crack sizes were determined by fracturing the specimens after the final ultrasonic measurement, photographing the crack surfaces, and measuring the crack dimensions from the high-resolution photographs. Each crack depth in the table is the average of the maximum depth measured on both sides of the hole. It should be noted that there are variations in the transducer mounting and hole geometry as compared to the procedures described in Section 2.1. In particular, in reference to Fig. 3, for some of the samples the transmitter and receiver were equidistant from the centre of the hole and different numbers of V paths were used. Also, some of the holes had a counterbore and countersink. Additional mounting variations were caused by difficulties in achieving perfect transducer positioning and alignment. These variations were not taken into consideration in determining the measurement model.

The procedure for calculating the empirical relationship between crack depth and the energy ratio response is similar to a probability of detection (POD) methodology[31]. Following the convention for POD, the flaw size variable is a (i.e., crack depth x) and the ultrasonic response is $\hat{a}$. Here $\hat{a}$ is taken to be one minus the energy ratio ($\hat{a} = 1 - \bar{R}$) so that increasing crack depths correspond to increasing values of $\hat{a}$. As with standard approaches for calculating POD curves, the intent is to find a functional relationship between $\hat{a}$ and a such that the residuals are normally distributed with a constant variance[31]. That is,

$$g(\hat{a}) = f(a) + \nu \quad \ldots (16)$$

where ν is a zero mean Gaussian random variable with variance σ_ν^2. Figure 8(a) shows a log-log presentation of the data of Table 1. A visual examination of the plot indicates that a linear relationship is appropriate and the constant variance assumption is reasonable. The points corresponding to the largest and smallest cracks were excluded, and the linear fit was obtained as,

$$\log_{10}(\hat{a}) = c_0 + c_1 \log_{10}(a), \quad \ldots (17)$$

where c_0 and c_1 are the data fitting parameters. This expression can also be given in the linear domain as

$$\hat{a} = 10^{c_0} a^{c_1}. \quad \ldots (18)$$

The linear fit is shown in the log-log plot of Fig. 8(a). Figure 8(b) shows the same information on a linear plot and in terms of the energy ratio $\bar{R}$ instead of $\hat{a}$. Switching back to the variable x for crack depth, the measurement model for the EKF application is therefore $B(x) = 1 - 10^{c_0}x^{c_1}$ and its inverse is $\tilde{B}(\bar{R}) = [(1 - \bar{R})/10^{c_0}]^{1/c_1}$.

The variance associated with the measurement model, Q_v, also needs to be determined. The standard deviation in the log-log domain, σ_ν, is assumed to be constant. The variance, Q_v, is determined by transforming σ_ν to the linear plane, and is given as

$$Q_v = [(0{\cdot}5)10^{c_0} x^{c_1}(10^{\sigma_\nu} - 10^{-\sigma_\nu})]^2 + \sigma_e^2, \quad \ldots (19)$$

where σ_e is the standard deviation of the noise associated the measurement process defined earlier. Figure 8(b) shows the evolution of Q_v in the linear plane, displaying reasonable agreement with the experimental values.

3.2.3 System model

The next modelling aspect is determining an appropriate model for fatigue crack propagation, which is used as the system model for the EKF. It is desirable that this model be differentiable and based on established mechanics theories. As such, Paris's power law is used as the system model[32]. Paris's equation defines the rate of crack

https://doi.org/10.1017/S0001924000003432 Published online by Cambridge University Press

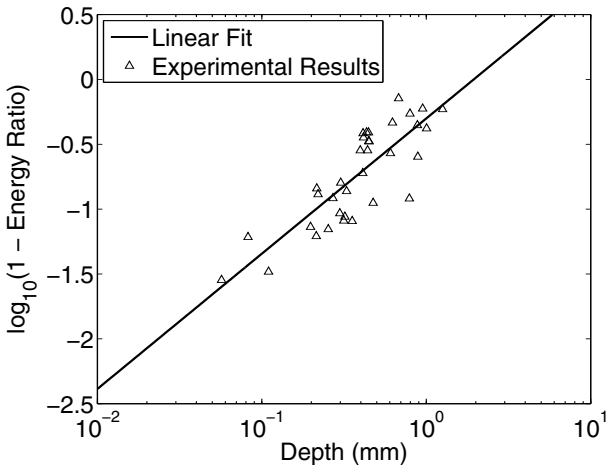

Figure 8. Raw data and linear fit of $\hat{a}$ *versus* a. (a) Log-log plot, and (b) linear plot.

growth as

$$\frac{\mathrm{d}x}{\mathrm{d}N_f} = C(\Delta K)^m, \qquad \ldots (20)$$

where x is the depth of a crack (and also the EKF state variable) and N_f is the number of fatigue cycles. As per Ref. 33, the material constants C and m for 7075 Al were taken to be $2{\cdot}71 \times 10^{-8}$MPa $\sqrt{\text{m}}$ and 3·7, respectively, with the resulting incremental growth rates in units of mm/cycle. The stress intensity range, ΔK, is given by

$$\Delta K = F\Delta S\sqrt{\pi x}. \qquad \ldots (21)$$

The applied stress range, or ΔS, is the difference between the high and low stress values for an individual fatigue cycle. For this study, it is assumed that the 2,640 cycle fatigue spectrum is known *a priori*. The choice of geometry correction factor, F, is based on the expected crack shape and crack growth process given the specimen geometry and fatigue process. A variety of geometry correction factors exist in the literature for cracks propagating from a notched specimen, such as through-thickness cracks[33], half circular cracks[34], and elliptical cracks[34,35]. For the work presented here, the parameter is defined as in Ref. 36,

$$F = F(x) = \frac{Q \cdot k_{\mathrm{T}}}{\sqrt{1 + 4.5 \cdot x/r}}, \qquad \ldots (22)$$

which assumes a hole of radius r with symmetric elliptical cracks of depth x and stress concentration factor k_T. For the specimen described in Section 2.2, the stress concentration factor is approximately 2·52. The Q variable captures the effect of different elliptical crack shapes, with Q = 0·65 corresponding to a half circular crack and Q = 1·12 corresponding to a through-thickness crack (an elliptical crack with very large aspect ratio). The system model, $A(x)$, and local linearisation, $\bar{A}(n-1)$, are then determined as

$$x(n+1) = A(x(n)) = x(n) + \sum_{i=1}^{\Delta N_f} C(\Delta K_i)^m, \qquad \ldots (23)$$

$$\bar{A}(n-1) = x(n) - x(n-1), \qquad \ldots (24)$$

where the summation is over the ΔN_f fatigue cycles between measurements. The ΔK_i parameter is the stress intensity range for the ith cycle of the 2,640 cycle fatigue spectrum. The summation explicitly accounts for the specific loading characteristics of each fatigue cycle.

The choice of Paris's power law for this problem was viable given the simple geometry and fatigue process, but other approaches are possible for approximating the crack growth process. Miner's Rule as well as modifications of Paris's power law, such as the Walker or Foreman equations, are additional examples of approximations of the crack growth process[33]. For more complex scenarios, such as multi-axis fatigue, complicated specimen geometries and composite structures, numerical codes such as FASTRAN[37] or NASGRO[38] could be used to capture the crack growth dynamics. Data-driven approximations[39] or component-level models[40] may also be viable if they adequately capture the effects of variable loading.

3.2.4 System model variance

The remaining Kalman filter parameter to quantify is the variance of the system model, Q_w. The original Paris's equation described in Section 3.3.2 is a deterministic equation. Practical experience, however, is that cracks grow differently for nominally identical specimens and loading, primarily because of variations in microstructure. The approach taken here for quantifying these variations is to randomise parameters of Paris's equation. Then, for a given crack depth and fatigue spectrum, multiple iterations of crack growth curves are computed using distributions of the randomized parameters, and the variance, Q_w, is calculated from the resulting distribution of the final crack depths.

Randomising the material constants of Paris's equation was proposed by Ray and Patankar[41], where they generated the multiplicative material constant, C, from a log-normal random distribution, Ω. Based upon their results, the expected value, $E[\Omega]$, and variance, Q_Ω, of the Ω distribution are

$$E[\Omega] = C, \qquad \ldots (25)$$

$$Q_\Omega = 7.91\times10^{8}\,\frac{C^2}{\Delta S^{2m}}, \qquad \ldots (26)$$

where ΔS is the stress intensity range and C and m are the material constants from before. Since the experiments for this study utilise spectrum loading, the ΔS for computing the variance is taken to be the average ΔS during the entire 2,640 cycle spectrum. For each iteration, the constant C is generated from this distribution.

The second variability between experiments is related to the crack shapes. Based on experience, likely crack shapes range from a single

https://doi.org/10.1017/S0001924000003432 Published online by Cambridge University Press

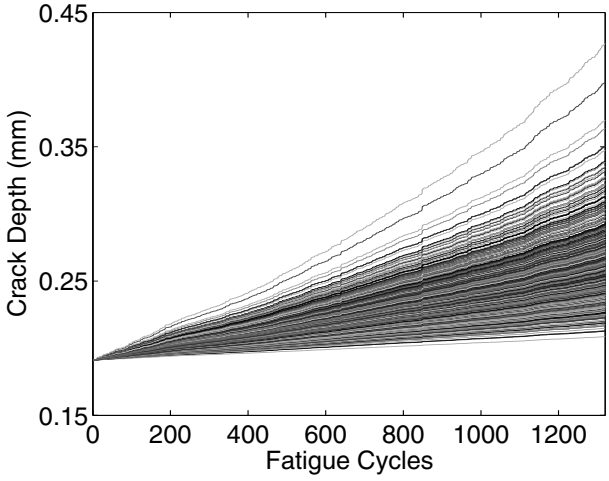

(a)

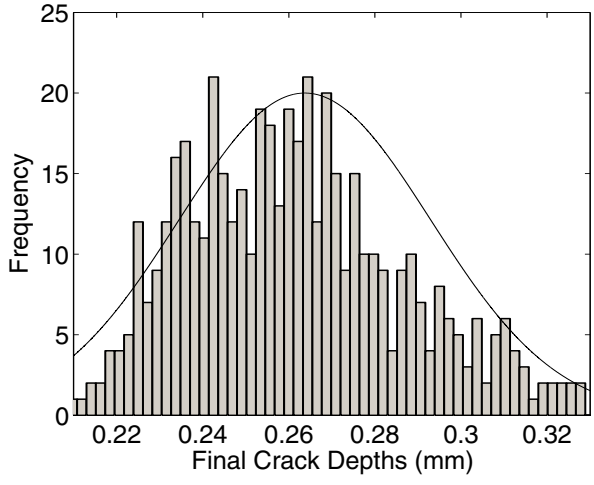

(b)

Figure 9. (a) Crack growth curves for computing the the crack depth variance, Q_w , for an initial crack size of approximately 0·2mm and a 1,320 cycle spectrum. (b) The corresponding histogram of final crack depths with a Gaussian curve shown for comparison.

half circular crack to a through-thickness crack; unions of multiple cracks give rise to intermediate shapes. Referring back to Equation (22), the shape variable, Q, is randomly generated from a normal distribution with a mean of 0·885 and a standard deviation of 0·0783. Six standard deviations of this distribution span the range between 0·65 and 1·12, which corresponds to elliptical cracks ranging from half circular to through-thickness.

Using the above methodology for computing the crack growth parameters, a total of 500 iterations of C and Q were used to compute the variance Q_w at each timestep of the EKF framework. As an illustration, consider a crack depth of 0·2mm fatigued by the 1,320 cycle spectrum. Figure 9(a) illustrates the range of expected crack growth curves, where Q_w is the variance of the final crack depths. Also, Fig. 9(b) shows the histogram of the final crack depths compared to a Gaussian curve with the same mean and variance as the final crack depths. Given that the approximation for the system model variance involves generating C from a log-normal distribution, the resulting distribution in final crack sizes after 2,640 fatigue cycles is not expected to be perfectly Gaussian. The pragmatic approach taken here is to assume that the deviation from a Gaussian distribution is not too severe and proceed with the EKF, which was done successfully in Refs 42 and 43 for other applications.

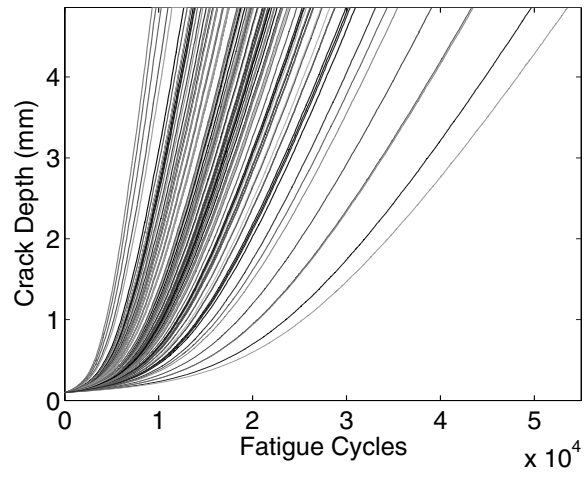

Figure 10. Example crack growth curves from the Monte Carlo simulation for a starting crack depth of 0·1mm.

3.3 Prognosis estimation

In parallel to the state estimation framework for tracking fatigue damage, an estimate of remaining life is generated using the crack growth model. A Monte Carlo simulation of expected crack growth curves is performed to estimate the distribution of fatigue cycles to reach a critical crack size, similar to the approach described by Hoffman and Hurtado[44]. Based on fatigue experience for the straight through-hole with no fastener, failure is imminent once the crack has reached the surface of the specimen and has grown approximately 2mm on the surface from the edge of the hole. Assuming a semi-circular crack front, this corresponds to a crack depth of 4·86mm ($h/2$ + 2mm where h = 5·72mm is the specimen thickness). The number of cycles it would take for the current crack to reach this critical depth is the definition of remaining life used here.

The process for computing the prognosis of remaining life is based on the randomised system model described in Section 3.2.4. For each prognosis computation, the EKF output is assumed to be the exact crack depth at that time. Although not done here, this simplification could be relaxed by first estimating a distribution of crack sizes. A Monte Carlo simulation is then performed by statistically varying the material constant C and shape parameter Q as previously described to produce a series of crack growth curves starting at the crack size determined by the Kalman filter. Example crack growth curves are shown in Fig. 10, which consists of 100 iterations of the Monte Carlo simulation starting at 0·1mm, where each curve stops after reaching 4·86mm, the point of expected failure. A total of 2,500 iterations of this process are performed and the number of cycles to reach the critical crack depth is computed. Figure 11 shows a typical distribution of remaining cycles to failure.

4.0 RESULTS

This section reports the performance of the entire methodology for detecting cracks, estimating their sizes, and predicting remaining life. A total of ten experiments were considered as described in Section 2.2. The material fatigued was 7075-T651 aluminium, the

https://doi.org/10.1017/S0001924000003432 Published online by Cambridge University Press

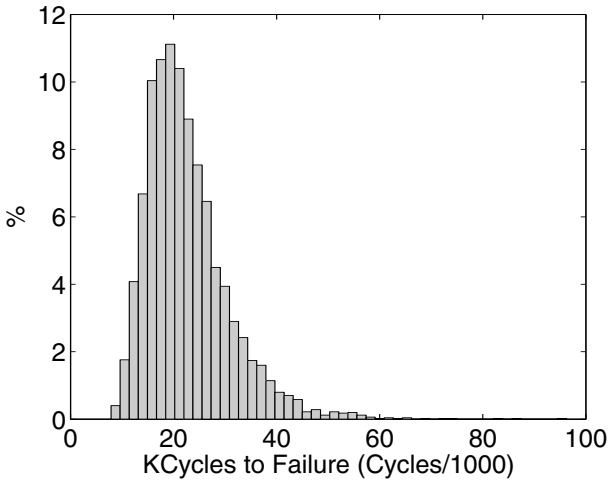

Figure 11. Example histogram showing the predicted distribution of remaining cycles until failure for a crack depth of 0·1mm and 5,000 iterations.

same as for the derivation of the system model for crack growth. No attempt was made to ensure symmetric cracking on both sides of the holes, even though symmetry is assumed for the system model (the crack growth relationship used for the EKF). The value of Q for the geometry correction factor (Equation (22)) was taken to be 1·0, which corresponds to cracks with a large aspect ratio, to best match the final crack sizes in a mean-absolute error sense. It should be noted that consideration of additional specimens, either empirically or via models, might result in a different value for Q.

Data from eight experiments were analysed to examine the efficacy of the proposed methodology for detecting and sizing defects. These data are from experiments #30-37 of Table 1, and were obtained using identical transducer configurations. Fatiguing was halted well before failure, and results from the combined detection and state estimation methodology are compared to a purely measurement-based approach.

Data from the ninth and tenth experiments were analysed to evaluate the ability of the prognosis strategy to predict the remaining structural life. For both of these experiments, the specimens were fatigued to failure. The ninth experiment is not included in Table 1 because it was not possible to measure the crack depth prior to failure. The tenth experiment corresponds to experiment #10 of Table 1. For this experiment the transducers were not removed until just a few cycles before failure, so the crack depth in the table was taken from the final fracture surface after failure.

4.1 Detection results

The energy ratio curves from each of the eight experiments for state estimation verification are shown in Fig. 12. As can be seen in the figure, the experiments were stopped at a variety of final crack sizes. Additionally, it should be noted that the energy ratio curves before detection typically exhibit small upward or downward slopes. This slope is thought to be related to both changes in the transducer coupling and permanent deformation (elongation) of the specimen. The energy ratio curves were renormalised to compensate for this trend by scaling the curves so that the maximum value before detection was unity. The renormalised curves are shown in Fig. 12, and it can be seen that the final energy ratios differ slightly from those shown in Table 1 for experiments #30-37. Finally, the output of the crack detection algorithm is highlighted on each curve by a triangular marker.

4.2 Crack size estimates from measurements

Crack sizes were first estimated from each energy ratio curve using only the inverse measurement model. This inverse model provides an estimate of the crack depth given the ultrasonic energy ratio; i.e., $x = \widetilde{B}(\bar{R})$. The resulting crack size estimates are shown as the dotted curves in Fig. 13 for each of the eight experiments. For consistency with the crack detection algorithm, it is assumed that there are no cracks prior to 19,000 cycles and thus results are shown from that point until fatiguing was halted. The final crack depth is shown for each experiment as a black diamond, where this depth is the average of the maximum depths measured on both sides of the hole. As can be observed, the growth of each crack is generally tracked, but the final crack size estimate is not always accurate. Also, experimental variations of the measurement process carry over into the measurement model response, which is particularly evident from the non-zero crack size estimates obtained prior to detection. These two effects serve as the justification for the state estimation framework given the preponderance of false alarms early in the fatigue process from measurement noise and unrealistic growth behaviour for the defect without incorporating a model for how a fatigue crack should evolve.

4.3 Tracking results

This section summarises the performance of the state estimation methodology for estimating crack sizes. For each experiment, the EKF framework response is compared to the results from the inverse measurement model. Estimates using only crack growth laws (i.e., the system model) are not provided because such estimates require assuming an initial crack depth, which is not available prior to detection. For the EKF implementation here, the system model was used to provide an estimate of crack growth only after the crack was detected as determined by the crack detection algorithm of Section 3.1.

As can be seen in Fig. 13, the crack size estimates obtained from combining the crack detection algorithm with the EKF sizing methodology are qualitatively superior to those obtained from the measurement-only approach. In particular, measurement variations are not carried over into the crack size estimates before detection, and have little effect on the estimates after detection. Since only the final crack dimension is known, it is not possible to quantitatively assess the EKF performance prior to the final measurement; the parameter of interest is crack depth, which is only measurable after fracture of the specimen. At the time of the final measurement, six of the eight experiments showed improved crack size estimates using the EKF framework as compared to the measurement-based approach. However, for two of these eight experiments, the measurement-based approach provided more accurate final crack size estimates. The median absolute error in final crack depth estimates for all eight experiments using the EKF approach was 0·073 mm as compared to 0·131 mm using the purely measurement-based approach.

4.4 Prognosis results

The final two experiments (ninth and tenth) serve to illustrate the effectiveness of the prognosis strategy for predicting the remaining cycles until failure. For experiment #9, a fastener was installed in one of the holes to ensure that only the other hole developed fatigue cracks. Fatiguing was halted when the energy ratio fell to about 0·4, the transducers and fasteners were removed, and fatiguing was continued until failure. The applied stress used in Equation (21) was taken to be that for a single open hole prior to removal of the fastener, at which point the stress was recalculated for two open holes. As previously mentioned, for experiment #10 the transducers were not removed until just a few cycles before failure. The prognosis estimates do not include the last data point acquired just prior to failure, where the energy ratio was near zero (i.e., 0·041).

https://doi.org/10.1017/S0001924000003432 Published online by Cambridge University Press

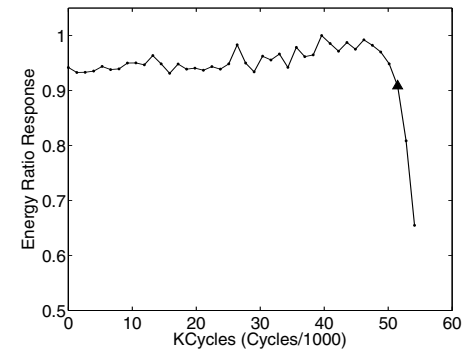

(a)

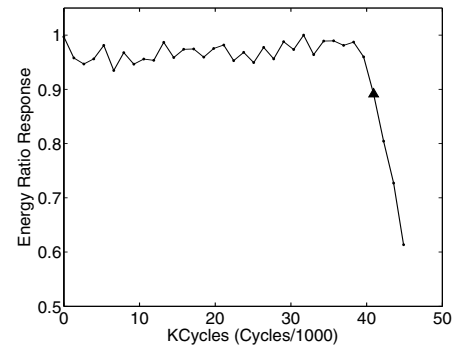

(b)

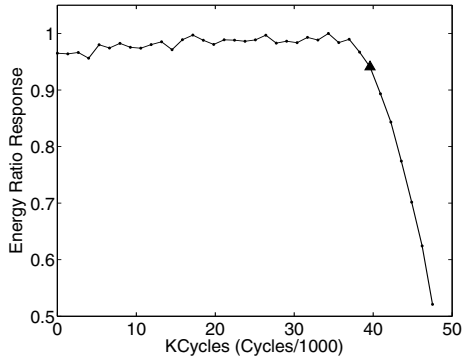

(c)

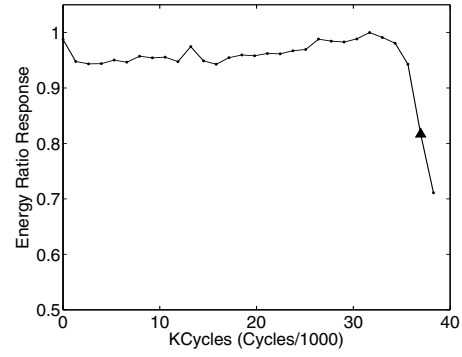

(d)

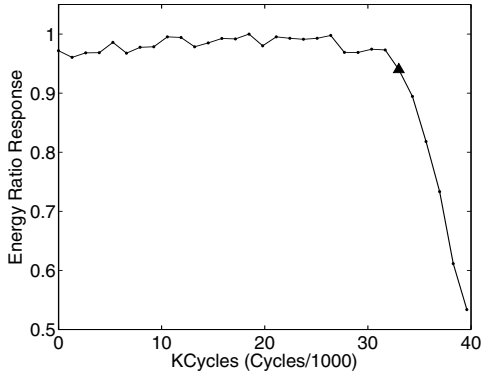

(e)

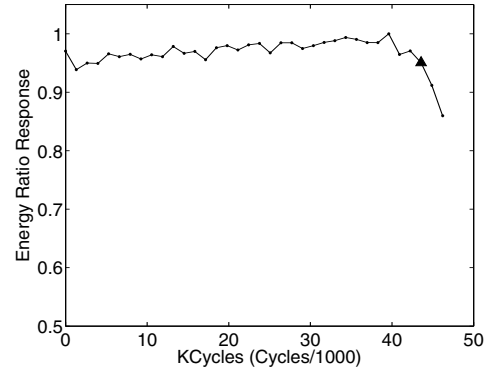

(f)

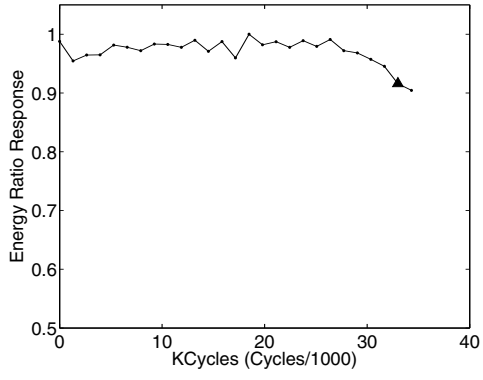

(g)

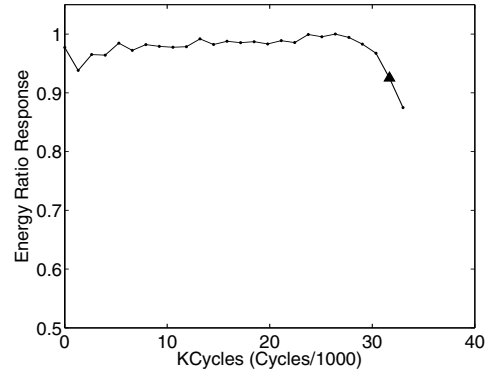

(h)

Figure 12. Energy ratio curves from the eight small crack experiments.
The measurement set corresponding to defect detection is highlighted by a triangular marker.

https://doi.org/10.1017/S0001924000003432 Published online by Cambridge University Press

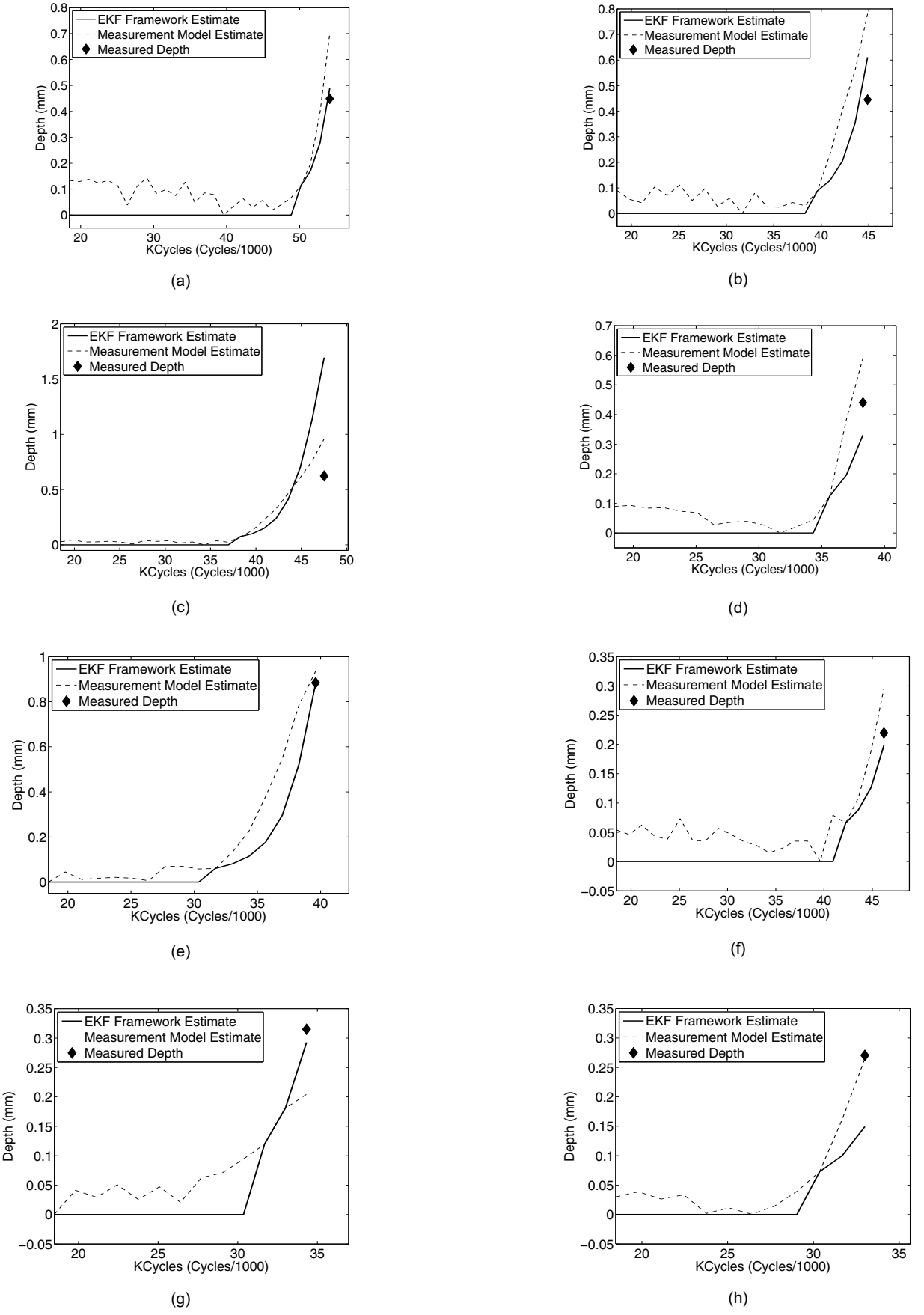

Figure 13. Results for the eight small crack experiments comparing estimated crack sizes from the inverse measurement model (dashed line) with those obtained from the SHM framework (solid line). The measured crack depth for each experiment is shown with a diamond marker.

https://doi.org/10.1017/S0001924000003432 Published online by Cambridge University Press

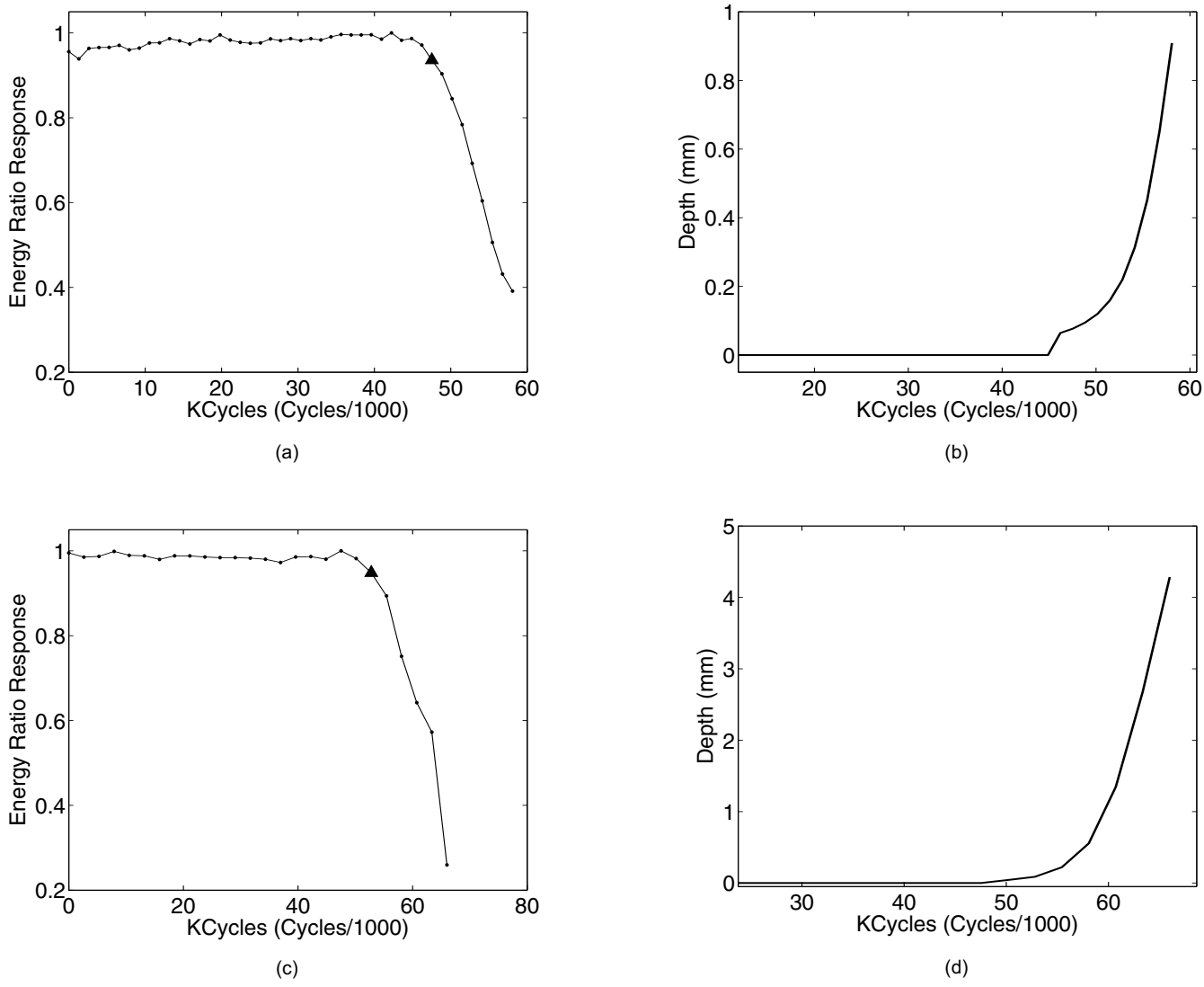

Figure 14. Data and results from the ninth (a,b) and tenth (c,d) experiments. (a,c) Normalised energy ratio curve with associated defect detection point. (b,d) Crack size estimates from the EKF framework.

For the ninth experiment, the resulting energy ratio curve is shown in Fig. 14(a), where the triangular marker indicates the point of crack detection. Data were recorded at an interval of 1,320 cycles, and the specimen failed at 69,500 cycles. Cracking is detected more than 20,000 cycles prior to failure, allowing eight energy ratio measurements to be processed with the EKF framework. Figure 14(b) presents the EKF crack sizing results, indicating that the estimated crack depth (average from both sides of the hole) is approximately 0·91 mm at the final ultrasonic measurement. In parallel with each EKF estimate, the total number of fatigue cycles to failure is estimated as a probability density function. Figure 15(a) summarises these results from the point of detection to the final ultrasonic measurement where the error bars correspond to the 10% and 90% points of the probability density function. As can be seen, the initial estimate for the total number of cycles to failure is about 82,000, which is an optimistic estimate of the remaining structural life compared to the true value of 69,500. Further, the associated error bars indicate a large uncertainty in this estimate. As additional measurements are acquired, the mean prognosis estimate moves closer to the true value and the error bounds decrease. The error bars indicate that the prognosis estimate is becoming more accurate as the fatigue process continues past detection. The final estimate of the total fatigue life has a mean of 75,180 cycles and error bars from 69,760 cycles to 85,030 cycles, which almost bracket the actual fatigue life of 69,500 cycles.

For the tenth experiment, there are several differences in the experimental setup compared to the ninth. First, no fastener was installed in either hole, although cracks were found to be present in only one hole. Further, the transducers were left on the specimen until very close to failure, which occurred at 67,600 cycles. Finally, data were collected every 2,640 cycles rather than every 1,320 cycles. The resulting energy ratio curve is shown in Fig. 14(c). As can be seen, the energy ratio curve drop is nearly 80%. Figure 14(d) presents the EKF crack sizing results, where the final crack size estimate is 4·3 mm. As before, the total number of fatigue cycles to failure is estimated as a probability density function and compared to 67,600 cycles. Figure 15(b) summarises these results for this experiment. Unlike for the first prognosis experiment, the error bars for the total fatigue life encompass the true value. As for the ninth experiment, as additional measurements are acquired, the mean prognosis estimate moves closer to the true value and the error bounds decrease. The final estimate of the total fatigue life has a mean of 67,340 cycles and the 10% to 90% error bars extend from 66,900 cycles to 68,140 cycles, which is in excellent agreement with the actual fatigue life of 67,600. The improved prognosis performance for this experiment compared to the previous

https://doi.org/10.1017/S0001924000003432 Published online by Cambridge University Press

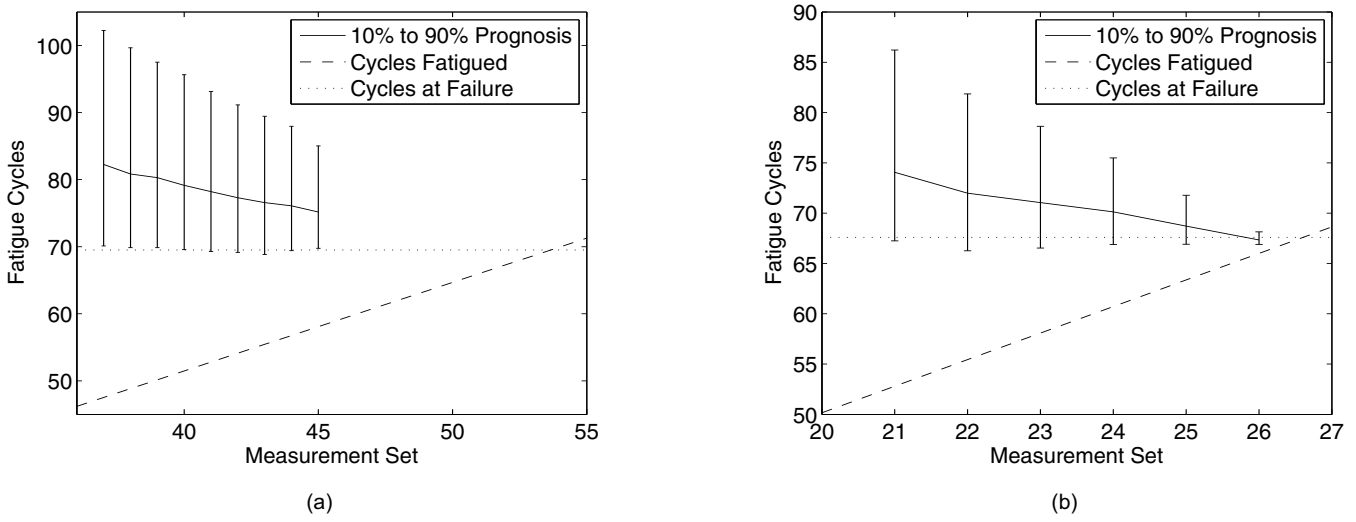

Figure 15. Prognosis results for the (a) ninth and (b) tenth experiments. Each prognosis estimate was determined from the state estimation output using the current measurement. The error bars correspond to the 10% and 90% percent points of the distribution of cycles to failure.

one is primarily a result of having measurement data available for larger crack sizes.

Since the specimens considered here were all fatigued at the same rate using the same spectrum loading, it would be possible to predict the remaining life after initial crack detection and growth using relatively simple curve fitting and extrapolation methods. However, this type of an approach is not extensible to the variable loads that are encountered under actual usage. The state estimation approach presented here, although not yet validated for variable loads, is formulated such that they can be readily considered.

5.0 SUMMARY AND CONCLUSIONS

This paper presents a framework for *in situ* ultrasonic monitoring of structural integrity using state estimation methodologies and demonstrates it on the problem of estimating sizes of fastener hole fatigue cracks in metallic components. This framework shows how time history data from permanently mounted ultrasonic sensors can be effectively used to improve both detection and sizing of fastener hole fatigue cracks. It further illustrates how noisy experimental data and approximate measurement and crack growth models can be integrated to achieve improved crack size estimates. A natural extension of this methodology is estimation of remaining structural life, or prognosis, which is also demonstrated here. Integral to the overall framework is an automated algorithm for detecting the presence of fatigue cracks, which allows for consistent detection of cracking while minimising the likelihood of noise causing a false alarm.

The sizing methodology presented here combines an ultrasonic measurement model with a classical crack growth relationship via a state estimation approach, specifically an extended Kalman filter. The variance of the ultrasonic measurement method has contributions from both variable crack geometries and random experimental variations. The measurement model and its associated variance were determined using an entirely empirical methodology. The variance of the crack growth model was approximated by estimating uncertainties in the material properties. It was found that the state estimation approach to crack sizing gives a better estimate of crack depth as compared to a purely measurement-based approach. The conclusion is that by combining the mechanisms for the progression of damage with the ultrasonic measurements, more accurate estimates of the degree of damage can be achieved. However, care must be taken to ensure that the crack growth and measurement models provide a reasonable representation of the target application, and that model and experimental uncertainties are reasonably well-characterised. Better models would likely improve performance, but the ultimate utility of this methodology may be its ability to provide useful results with simpler but less accurate models.

Presented here is only one possible approach to the problem of estimating both fatigue crack severity and remaining life of an aluminium fatigue coupon. For a more realistic structure, it may be necessary to use different sensor technologies, such as ultrasonic guided waves, eddy current methods, and acoustic emission, or combinations of these techniques to provide a more robust result. Furthermore, the modelling strategies for both measuring the crack size and approximating the crack propagation may need to be improved for complex geometries and fatigue processes. As an example, multiple sensor responses, from either different technologies or several signal features from a single technology, could be leveraged together to provide a better estimate of the size of the defect. Finally, more advanced state estimation approaches, such as particle filtering, may be required depending on the knowledge and complexity of the statistics related to the measurement methods and crack growth process.

The work here serves as an illustration of a general approach to ultrasonic structural health monitoring where the key differences between SHM and NDE are considered from the outset — the availability of time history data and the inability to move sensors. Optimisation of any ultrasonic SHM method must incorporate both of these characteristics rather than treating each data point as an individual inspection result. Explicitly incorporating damage growth mechanisms is one fundamental way of ensuring that time history data are analysed in a way that produces results consistent with known patterns of damage progression, and modelling of the measurement process ensures that the effects of crack geometry variations are statistically captured. This approach moves the field of SHM away from the mentality of single measurements and toward its inclusion as an integral part of an overall prognosis strategy.

ACKNOWLEDGMENTS

The authors gratefully acknowledge the support of the Defense Advanced Research Projects Agency (DARPA), Defense Sciences Office, Structural Integrity Prognosis System Program, contract No. HR0011-04-0003 to Northrop Grumman Corporation, Integrated Systems. This paper is approved for public release, distribution unlimited.

REFERENCES

1. THOMPSON, R.B. and THOMPSON, D.O. Ultrasonics in nondestructive evaluation, 1985, *Proceedings of the IEEE*, **73**, (12), pp 1716-1755.
2. GROOTEMAN, F. A stochastic approach to determine lifetimes and inspection schemes for aircraft components, *Int J of Fatigue*, 2008, **30**, pp 138-149.
3. ROSE, J.L. and SCHLEMM, H. Equivalent flaw size measurements and characterization analysis, *Materials Evaluation*, 1976, **34**, pp 1-8.
4. SILK, M.G. The transfer of ultrasonic energy in the diffraction technique for crack sizing, *NDT Int*, 1976, **9**, pp 290-297.
5. RAVENSCROFT, F.A., NEWTON, K. and SCRUBY, C.B. Diffraction of ultrasound by cracks: comparison of experiment with theory, *Ultrasonics*, 1991, **29**, pp 29-37.
6. SILK, M.G. The determination of crack penetration using ultrasonic surface waves, *Ultrasonics*, 1979, **17** , pp 113-120.
7. COOK, D.A. and BERTHELOT, Y.H. Detection of small surface breaking fatigue cracks in steel using scattering of Rayleigh waves, *NDT&E Int*, 2001, **34**, pp 483-492.
8. KELLER, E. and RAY, A. Real-time health monitoring of mechanical structures, *Structural Health Monitoring*, 2003, **2**, (3), pp 191-203.
9. MI, B., MICHAELS, J.E. and MICHAELS, T.E. An ultrasonic method for dynamic monitoring of fatigue crack initiation and growth, *J Acoustical Soc of America*, 2006, **119**, (1), pp 74-85.
10. KIM, J.-Y., YAKOVLEV, V.A. and ROKHLIN, S.I. Surface acoustic wave modulation on a partially closed fatigue crack, *J Acoustical Soc of America*, 2004, **115**, (5), pp 1961-1972.
11. HARRI, K. GUILLAUME, P. and VANLANDUIT, S. On-line monitoring of cracks using ultrasonic 'multisine' surface waves, 2006, Proceedings of the 9th European Conference on Non-Destructive Testing, pp Th.1.5.3:1-7.
12. CHANG, Z. and MAL, A. Scattering of Lamb waves from a rivet hole with edge cracks, *Mechanics of Materials*, 1999, **31**, (3), pp 197-204.
13. FROMME, P. and SAYIR, M. Detection of cracks at rivet holes using guided waves, *Ultrasonics*, 2002, **40**, (2), pp 199-203.
14. JARMER, G.J.S. and TODD, M.D. Crack detection diagnostics using ultrasonic insonification and pattern recognition, KUNDU, T. (Ed), Proceedings of SPIE, *Health Monitoring and Smart Nondestructive Evaluation of Structural and Biological Systems III*, 2009, **7295**, SPIE, Bellingham, Washington, pp 72950T:1-8.
15. STASZEWSKI, W.J., LEE, B.C. and TRAYNOR, R. Fatigue crack detection in metallic structures with Lamb waves and 3D laser vibrometry, *Measurement Science and Technology*, 2007, **18**, 187, pp 727-739.
16. LU, Y., YE, L., SU, Z. and HUANG, N. Quantitative evaluation of crack orientation in aluminum plates based on Lamb waves, *Smart Materials and Structures*, 2007, **16**, pp 1907-1914.
17. MICHAELS, J.E., MICHAELS, T.E. and MARTIN, R.S. Analysis of global ultrasonic sensor data from a full scale wing panel test, THOMPSON, D. O. and CHIMENTI D.E. (Eds), *Review of Progress in Quantitative Nondestructive Evaluation*, 2009, **28A**, American Institute of Physics, New York, pp 950-957.
18. COBB, A.C. MICHAELS, J.E. and MICHAELS, T.E. An automated time frequency approach for ultrasonic monitoring of fastener hole cracks, *NDT&E International*, 2007, **40**, pp 525-536.
19. GUPTA, S., RAY, A. and KELLER, E. Symbolic time series analysis of ultrasonic data for early detection of fatigue damage, *Mechanical Systems and Signal Processing*, 2007, **21**, pp 866-884.
20. GUPTA, S., RAY, A. and KELLER, E. Online fatigue damage monitoring by ultrasonic measurements: A symbolic dynamics approach, *Int J of Fatigue*, 2007, **29**, pp 1100-1114.
21. RAY, A. and TANGIRALA, S. Stochastic modeling of fatigue crack dynamics for on-line failure prognosis, *IEEE Transactions on Control Systems Technology*, 1996, **4**, (4), pp 443-451.
22. ORCHARD, M.E. and VACHTSEVANOS, G.J. A particle filtering approach for on-line prognosis in a planetary gear plate, *Int J of Fuzzy Logic and Intelligent Systems*, 2007, **7**, (4), pp 22-227.
23. KULKARNI, S.S., SUN, L., MORAN, B., KRISHNASWAMY, S. and ACHENBACH, J.D. A probabilistic method to predict fatigue crack initiation, *Int J of Fracture*, 2006, **137**, pp 9-17.
24. KULKARNI, S.S. and ACHENBACH, J.D. Strutural health monitoring and damage prognosis in fatigue, *Structural Health Monitoring*, 2008, **7**, (1), pp 37-49.
25. MICHAELS, J.E., MICHAELS, T.E. and MI, B. An ultrasonic angle beam method for in situ sizing of fastener hole cracks, *J Nondestructive Evaluation*, 2006, **25**, (1), pp 3-16.
26. MICHAELS, J.E., MICHAELS, T.E., COBB, A.C. and KACPRZYNSKI, G.J. Ultrasonic sensing and life prediction for the DARPA structural integrity prognosis system, in: THOMPSON, D.O. and CHIMENTI D.E. (Eds), *Review of Prog in Quantitative Nondestructive Evaluation*, 2006, **26B**, American Institute of Physics, New York, pp 1453-1460.
27. PAPAZIAN, J., SILBERSTEIN, R., WELSH, G., GRUNDY, D., CRAVEN, C., EVANS, L., GOLDFINE, N., MICHAELS, J., MICHAELS, T., LI, Y. and LAIRD, C. Sensors for monitoring early stage fatigue cracking, *Int J Fatigue*, 2007, **29**, pp 1668-1680.
28. MICHAELS, T.E., MICHAELS, J.E. and COBB, A.C. Simultaneous ultrasonic monitoring of crack growth and dynamic loads during a full scale fatigue test of an aircraft wing, THOMPSON, D.O. and CHIMENTI, D.E. (Eds), *Review of Prog in Quantitative Nondestructive Evaluation*, 2009, **28B**, American Institute of Physics, New York, pp 1458-1465.
29. MOON, T.K. and STIRLING, W.C. *Mathematical Methods and Algorithms for Signal Processing*, 2000, 1st Edition, Pearson Education.
30. HAYES, M. *Statistical Digital Signal Processing and Modeling*, 7th Edition, 1996, John Wiley and Sons.
31. MIL-HDBK-1823, Nondestructive evaluation system reliability assessment, 1999, Department of Defense.
32. PARIS, P. and ERDOGAN, F. A critical analysis of crack propagation laws, *J Basic Eng*, 1963, **85**, pp 528-534.
33. DOWLING, N.E. *Mechanical Behavior of Materials*, 10th Edition, 1993, Prentice-Hall, New Jersey.
34. SHAH, R.C. Stress intensity factors for through and part-through cracks originating at fastener holes, *Mech Crack Growth*, 1976, ASTM STP 590, ASTM, Philadelphia, pp 429-459.
35. MURAKAMI, Y. (Ed). *Stress Intensity Factors Handbook*, 1987, Pergamon Press, Oxford, UK.
36. LUCÁŠ, P. Stress intensity factor for small notch-emanated cracks, *Eng Fracture Mech*, 1987, **26**, (3), pp 471-473.
37. NEWMAN, J.C. Jr Fatigue-life prediction methodology using a crack-closure methodology, *J Eng Materials and Tech*, 1995, **117**, pp 433-439.
38. SKORUPA, M., MACHNIEWICZ, T., SCHIJVE, J. and SKORUPA, A. Application of the strip-yield model from the NASGRO software to predict fatigue crack growth in aluminium alloys under constant and variable amplitude loading, *Engineering Fracture Mech*, 2007, **74**, pp 291-313.
39. MOHANTY, S., DAS, S., CHATTOPADHYAY, A. and PERALTA, P. Gaussian process time series model for life prognosis of metallic structures, *Int J Intelligent Material Systems and Structures*, 2009, **20**, pp 887-896.
40. HAROON, M. and ADAMS, D.E. Development of component-level damage evolution models for mechanical prognosis, *J Applied Mech*, 2008, 75, pp 021017:1-15.
41. RAY, A. and PATANKAR, R. A stochastic model of fatigue crack propagation under variable-amplitude loading, *Eng Fracture Mech*, 1999, **62**, pp 477-493.
42. HILANDS, T.W. and THOMOPOULOS, S.C. A. Nonlinear filtering methods for harmonic retrieval and model order selection in Gaussian and non-Gaussian noise, *IEEE Transactions on Signal Processing*, 1997, **45**, (1), pp 982-995.
43. JETTO, L. LONGHI, S. and VENTURINI, G. Development and experimental validation of an adaptive extended Kalman filter for the localization of mobile robots, *IEEE Transactions on Robotics and Automation*, 1997, **15**, (2), pp 219-229.
44. HOFFMAN, P. and HURTADO, J. Airframe integrity based on Bayesian approach, 2006, Proceedings of the Annual Reliability and Maintainability Symposium, pp 630-635, IEEE, Piscataway, New Jersey.